Integrated omics networks reveal the temporal signaling events of brassinosteroid response in *Arabidopsis*

Natalie M Clark[1], Trevor M Nolan[2,4], Ping Wang[2], Gaoyuan Song[1], Christian Montes[1], Hongqing Guo[2], Rosangela Sozzani[3], Yanhai Yin[2], and Justin W Walley[1,✉]

[1]Department of Plant Pathology and Microbiology, Iowa State University, Ames, IA 50011
[2]Department of Genetics, Developmental, and Cell Biology, Iowa State University, Ames, IA 50011
[3]Department of Plant and Microbial Biology, North Carolina State University, Raleigh, NC 27695
[4]Current Address: Department of Biology, Duke University, Durham, NC 27708, USA

Brassinosteroids (BRs) are plant steroid hormones that are known to regulate cell division and stress response. We used a systems biology approach to integrate multi-omic datasets and unravel the molecular signaling events of BR response in *Arabidopsis*. We profiled the levels of 32,549 transcripts, 9,035 protein groups, and 26,950 phosphorylation sites from *Arabidopsis* seedlings treated with brassinolide (BL, most active BR) for six different lengths of time. We then constructed a network inference pipeline called Spatiotemporal Clustering and Inference of Omics Networks (SC-ION) that was able to integrate these multi-omic data into one, cohesive regulatory network. Our network illustrates the signaling cascade of BR response, starting with kinase-substrate phosphorylation and ending with transcriptional regulation. We used our network predictions to identify putative, relevant phosphorylation sites on the TF BRI1-EMS-SUPPRESSOR 1 (BES1); the importance of which we experimentally validated. Additionally, we identified an uncharacterized TF, which we named BRONTOSAURUS (BRON), that regulates cell division. Further, we show that *bron* mutant roots are hypersensitive to BL. Together, this work demonstrates the power of integrative network analysis applied to multi-omic data and provides fundamental insights into the molecular signaling events occurring during BR response.

multi-omics | regulatory network | brassinosteroid
Correspondence: *jwalley@iastate.edu*

Introduction

Brassinosteroids (BRs) are involved in a number of important biological processes including cell elongation and division, photomorphogenesis, reproduction, and both biotic and abiotic stress responses. The BR signaling pathway has been well-established in *Arabidopsis* (23, 39, 41). BRs are first sensed by the plasma membrane-localized receptor BRASSINOSTEROID INSENSITIVE 1 (BRI1) (11, 17, 24). Upon BR binding, BRI1 recruits co-receptors including BRI1-ASSOCIATED RECEPTOR KINASE 1 (BAK1) that are required for its activation (26, 36). In the absence of BR, the GSK3 kinase BRASSINOSTEROID INSENSITIVE 2 (BIN2)

phosphorylates numerous substrates including the transcription factors (TFs) BRI1-EMS-SUPPRESSOR 1 (BES1) and BRASSINAZOLE-RESISTANT 1 (BZR1) (16, 25, 36, 63, 66). This phosphorylation inactivates BES1/BZR1 through cytoplasmic retention, degradation and/or reduced DNA binding. When BRs are present, the BRI1/BAK1 complex activates a kinase signaling cascade resulting in the inactivation of BIN2 and the dephosphorylation of BES1/BZR1. This allows BES1/BZR1 to regulate target gene expression in the nucleus (15, 40, 49, 57, 62–64). While there are many conserved GSK3 phosphorylation sites in BES1/BZR1 proteins, the exact sites that are phosphorylated by BIN2 and the sites responsible for negative regulation of BES1 activity are not well defined.

The role of BR in modulating cell division is well-documented, particularly in the *Arabidopsis* root. It has been shown that BL has a dose-dependent effect on cell division in the root meristem: roots treated with higher levels of BL have more meristematic cells. Additionally, the *bes1-D* gain-of-function and *bri1-116* loss-of-function mutants have altered cell cycle progression, which implicates that plant cyclins may be involved. Accordingly, it has been shown that CYCLIN D3;1 (CYCD3;1) is induced by BL and can rescue cell division defects in the *bri1-116* mutant (14, 19). BR has also been implicated in stem cell division and maintenance: roots treated with BL have excessive QC divisions and altered expression patterns of QC cell identity markers (14, 30, 53).

The BR signaling pathway in *Arabidopsis* is highly dependent on the levels of protein phosphorylation, modulation of protein levels, and downstream transcriptional regulation. Therefore, we determined the dynamic response to BR signaling in *Arabidopsis* by performing large-scale transcriptome and (phospho)proteome profiling of seedlings treated with BL for different lengths of time. We then inferred a set of integrated, TF-centered Gene Regulatory Networks (GRNs) using our newly-developed Spatiotemporal Clustering and Inference of Omics Networks (SC-ION) pipeline. These networks illustrated how the phosphorylation state of TFs is important for predicting their downstream target genes. Additionally, SC-ION allowed us to infer one network per time point and visual-

ize the early and late (phospho)protein-transcript regulations in BR response. By combining these TF-centered networks with a correlation-based kinase signaling (i.e. kinase-centered) network, we illustrated the temporal cascade of BR response starting with kinase signaling and ending with differential transcript abundance. We were able to use this network to predict and experimentally validate previously uncharacterized BIN2 phosphorylation sites on BES1. Additionally, through network motif analysis, we identified a number of TFs putatively involved in BR response. In particular, we identified a C2H2-like TF whose mutants displayed hypersensitivity to BR, longer roots, and more cell divisions. The combination of this mutant's developmental phenotype as well as its putative role in BR response led us to name this TF BRONTOSAURUS (BRON). Together our results provide a comprehensive guide to molecular signaling changes that occur in response to BR.

Results

Generating an integrative omics dataset of temporal BR response. To investigate the temporal response to BRs, we established a treatment system in which seedlings were sensitized to BRs by pre-treatment with 1 µM of the BR biosynthesis inhibitor brassinazole (BRZ) (3) for 7 days to reduce background BR signaling. The 7-day-old seedlings were then treated with a mock solvent or 1 µM BL for six different lengths of time (15 min, 30 min, 1 hr, 2 hr, 4 hr, 8 hr) (Fig 1A) . To confirm efficacy of the BL treatment, we assayed BES1 by western blot (Fig. S1). In BRZ treated seedlings, we found that BES1 predominantly exists in its phosphorylated form, while BL-treated seedlings showed an accumulation of dephosphorylated BES1 over time. Specifically, we observed an increase in the amount of dephosphorylated BES1 as early as 15 minutes after treatment, and the phosphorylated form of BES1 was undetectable by 1 hour after treatment (Fig. S1). This demonstrates the expected BES1 response and thus the efficacy of BL treatment.

Based on the dynamic nature of BL response, we expected many transcripts, proteins, and phosphosites would have differential responses depending on the length of BL treatment. Thus, we performed multi-omics profiling of BL-treated and mock-treated seedlings at each of the six timepoints (Fig 1A). We used 3' QuantSeq (35) to measure transcript levels and quantified protein abundance and phosphorylation level by performing two-dimensional liquid chromatography-tandem mass spectrometry (2D-LC-MS/MS) on Tandem Mass Tag (TMT) labeled peptides (18, 32, 46–48).

To facilitate analysis of complex multi-run proteomics datasets, we constructed an analysis pipeline for quantitative proteomics data called TMT Normalization, Expression Analysis, and statistical Testing (TMT-NEAT). Our pipeline, which works on data generated from any organism, takes the TMT reporter ion intensity values (i.e. MaxQuant proteinGroups or PTM_Sites) and a metadata file containing sample information and TMT-labeling scheme as input. It first cleans the data by removing contaminants and appropriately labels the intensity data using the metadata file. Second, TMT-NEAT performs sample loading (within-run) and internal reference (between-run) normalization to eliminate batch effects (42). Third, it provides multiple qualitative plots such as hierarchical clustering and principal component analysis to visualize differences between biological groups. Finally, it performs differential expression analysis on the normalized values using a user-supplied *p*- or *q*-value threshold (Fig 1B). TMT-NEAT is publicly available and can be run through an RShiny Graphical User Interface (GUI) (see Methods).

Using these methods, we identified 32,549 transcripts, 9,035 protein groups, and 26,950 phosphosites (arising from 5,648 phosphoproteins) across the six timepoints (Fig 1C, Datasets S1-S3). We found that the number of differentially expressed (DE) transcripts, proteins, and phosphosites varied depending on the time point. When we examined the transcript data, we found that only 208 transcripts (17 up, 191 down) were DE in response to BL within the first 15 minutes, whereas 454 protein groups (214 up, 250 down) and 590 phosphosites (237 up, 353 down) were DE at this same time point. In addition, many more transcripts (2,653 total: 1,247 up, 1,406 down) were DE beginning at 30 minutes, which led us to speculate that the early BR response is predominantly post-transcriptional. This is supported by the role of BES1/BZR1, which must be dephosphorylated in order to enter the nucleus and transcriptionally regulate downstream genes in response to BR (16, 62, 63).

We next performed Gene Ontology (GO) analysis on the DE transcripts, proteins, and phosphosites at early (1 hour or earlier) and late (after 1 hour) timepoints (Fig S1, Dataset S4). We found that multiple BR response terms are enriched at different time points and for different DE gene-products. For example, BR mediated signaling pathway and cellular response to BR stimulus terms are enriched in the DE phosphosites at both early and late time points. Additionally, BR biosynthetic process and BR homeostasis are enriched in the DE transcripts at early timepoints, and the term for response to brassinosteroid is enriched in both DE transcripts and phosphosites. We also see enriched terms that have been linked to BR response such as cellular response to stress, response to auxin mediated signaling pathway, and defense response (38). Taken together, our omics profiling captures how different gene products temporally respond to BR treatment in *Arabidopsis*.

Predictive networks illustrate the temporal cascade of BR response. We have previously shown that integrating mRNA, protein, and phosphorylation data sets greatly

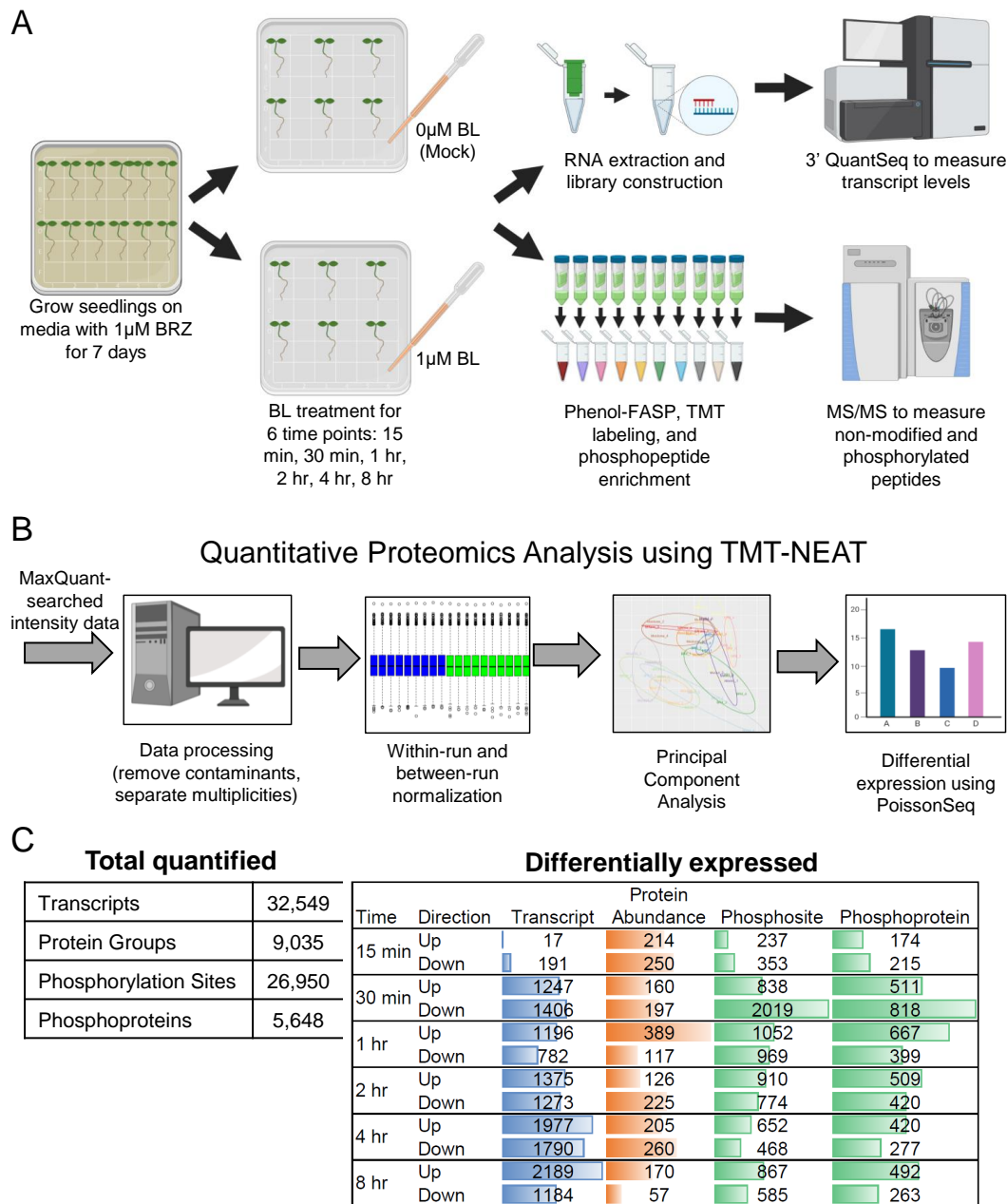Clark *et al.* | Integrated networks of brassinosteroid response

Fig. 1. An integrated omics time course of BR response. (A) Samples were collected at six time points (15min, 30min, 1hr, 2hr, 4hr, 8hr) from Mock and BL treated seedlings. (B) TMT-NEAT analysis pipeline for quantitative proteomics. (C) (left) Total number of transcripts, proteins, and phosphosites/phosphoproteins quantified at each time point. (right) Number of DE transcript, proteins, and phosphosites/phosphoproteins at each time point. Colored bars represent the relative number of DE gene-products within each data type.

improves the predictive power of reconstructed gene regulatory networks (GRNs) (54). However, integrating these multi-omics data types remains challenging. Thus, we next developed a network inference pipeline, which we named Spatiotemporal Clustering and Inference of Omics Networks (SC-ION), to integrate any number of different types of expression profiles into one cohesive, predictive GRN (Fig. 2A, see Methods). SC-ION builds on our MATLAB-based pipeline Regression Tree Pipeline for Spatial, Temporal, and Replicate data (RTP-STAR)

(7, 65), which is an adaptation of the GENIE3 (20) network inference method and functions only on transcriptomic datasets. In SC-ION, we further improve on RTP-STAR by: 1) incorporating Dynamic Time Warping (DTW) clustering for temporal data (13) and Independent Component Analysis (ICA) clustering for non-temporal data (37); 2) allowing the user to provide separate regulator and target matrices for integration of DE gene-products; 3) integrating any number of different types of expression profiles into one GRN; and 4) providing our pipeline as an
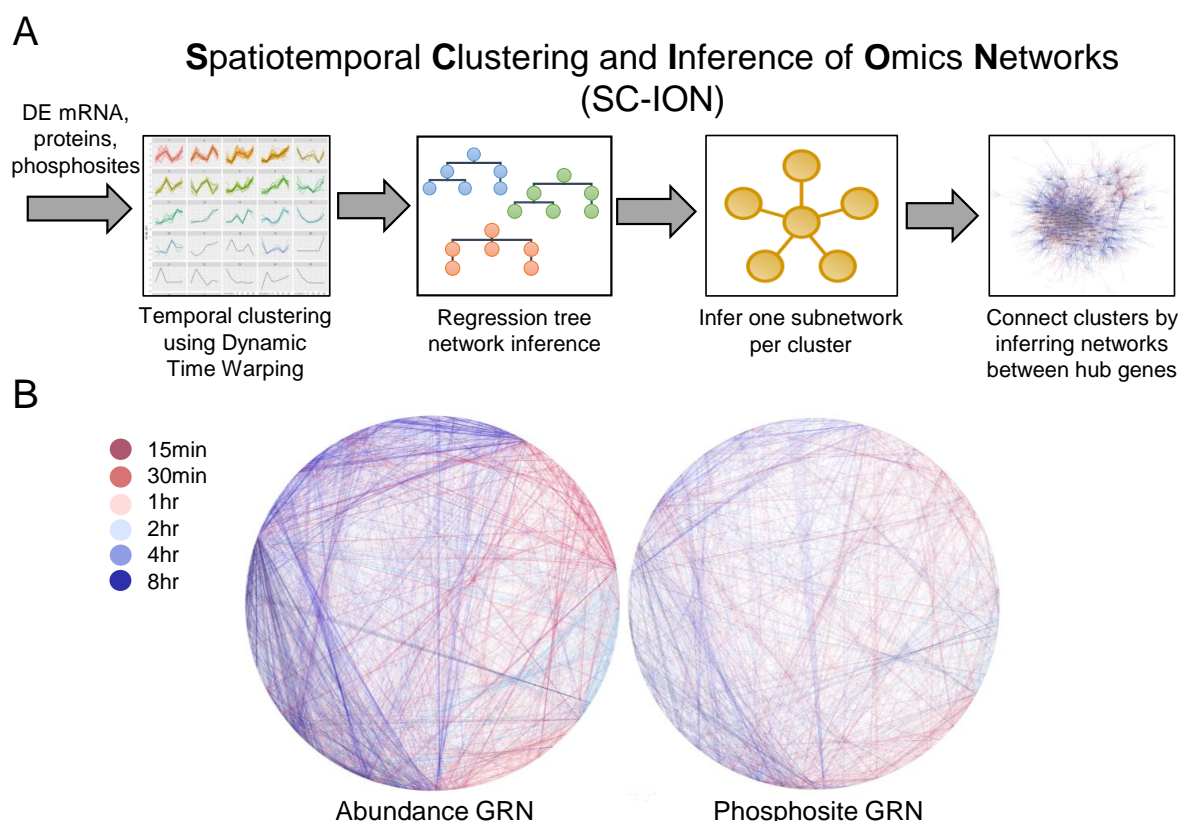
A

Spatiotemporal Clustering and Inference of Omics Networks (SC-ION)

DE mRNA, proteins, phosphosites → Temporal clustering using Dynamic Time Warping → Regression tree network inference → Infer one subnetwork per cluster → Connect clusters by inferring networks between hub genes

B

15min
30min
1hr
2hr
4hr
8hr

Abundance GRN   Phosphosite GRN

Fig. 2. Time-point-specific, integrative omics networks of BR response. (A) SC-ION pipeline. (B) Time-point-specific networks using TF abundance (left) or TF phosphosite intensity (right). Edge color represents the time point that regulation is predicted to occur.

RShiny GUI (Fig. 2A).

Here, we used SC-ION to infer two separate transcription factor (TF)-centered networks of BR response. In these TF-centered GRNs, TFs serve as "regulators" used to infer their "target" genes. In the first network, which we call the abundance network (blue, solid edges, Fig 3), TF protein abundance (when quantified) or TF transcript abundance (when cognate protein was not quantified) was used as the "regulator" value to infer their "target" transcript abundance. In the second phosphosite network (green, dashed edges, Fig 3), we inferred the "target" transcript abundance using TF phosphosite intensities as the "regulator" value. For each of these networks, we took advantage of our temporal data by 1) clustering the gene-products using DTW to create temporally-informed regulatory modules and 2) inferring one network per time point to visualize the regulations unique to each time point (Fig 2B). When connecting the time-point-specific networks, we found that there were distinct clusters of early and late predictions. In addition, there is cross-communication between the time points, where early regulators feed-forward into late regulators, and conversely where late regulators feed-back onto early regulators (Fig 2B).

In addition to our SC-ION-generated TF-centered GRNs,

we used our correlation-based approach to infer a kinase signaling network (purple, dotted edges, Fig 3) (55). In this network, we considered kinases with DE phosphosites in their p-loop (also termed activation loop) domain as potential regulators, as these phosphorylated kinases should be active (1) and thus useful for predicting kinase-signaling (4, 44, 55). In agreement with our previous work in maize (55), we observed that the correlation between kinase protein abundance and kinase p-loop phosphorylation intensity (i.e. activation state) greatly varies depending on the time point (Fig S3), motivating our use of p-loop site intensities rather than simply kinase abundance in our network. This "kinase-centered" network complements our TF-centered GRNs by predicting kinase-dependent signaling events.

When we merged our kinase signaling network with our TF-centered networks, we found that genes with known roles in the BR response pathway (39) were significantly enriched in the list of network regulators (Hypergeometric test, p<0.001). Additionally, we noticed that this merged network illustrates the temporal cascade of BR response across these different omics levels (Fig. 3, Dataset S4). Our inferred network places the kinase signaling interactions (purple) towards the top of the network (early in time). Next are the TF phosphosite-level regulations (green), followed by the TF abundance-level regulations (blue). Thus,
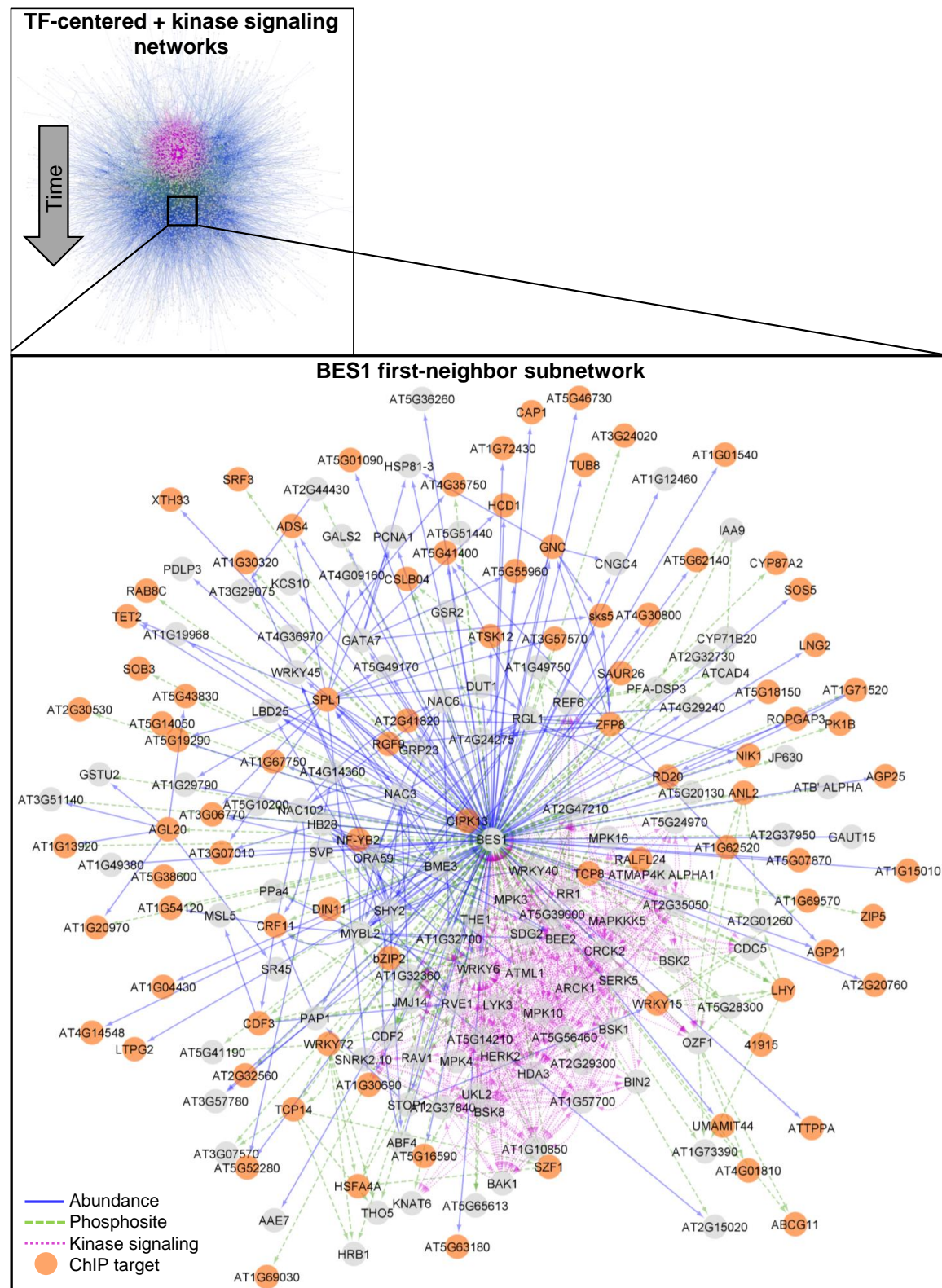
Fig. 3. Integration of TF-centered and kinase signaling networks. (Top) Merged networks. TF-abundance, blue solid; TF-phosphosite, green dashed; kinase signaling, purple dotted. The network is arranged temporally, with early regulations at the top and later regulations towards the bottom. (Bottom) First-neighbor subnetwork of BES1. Genes are gray circles, and size of genes corresponds to Normalized Motif Score. Orange genes are BES1/BZR1 ChIP-Seq targets.

our network predicts that BR response begins with kinase signaling, followed by transcriptional regulation via modulation of TF phosphorylation and/or abundance. This network prediction is in agreement with what we currently know about BR signaling, which begins with the kinases BRI1 and BAK1 initiating a series of (de)phosphorylation events leading to the regulation of downstream target genes by TFs including BES1 and BZR1. Our timepoint-specific networks further illustrate which regulations are predicted to occur in early or late BR response (Fig 2B).

Integration of kinase-signaling and TF-centered networks reveals the BIN2-BES1 signaling cascade in response to BR. We extracted the first-neighbor network of BES1 to illustrate how our multi-omics profiling and integrative network inference can elucidate the signaling events that occur in response to BR (Fig. 3). This network contains kinases that are predicted to be upstream of BES1 phosphorylation, TFs that are predicted to transcriptionally regulate BES1, and downstream targets of BES1. Our kinase-signaling network predicted that Serine 179 and Serine 180 (S179, S180) on BES1 are downstream of known BR-responsive kinases such as BIN2, BAK1, and BSK1 (16, 26, 50) (Fig S3). In addition, while not present in our kinase signaling network, S171 differentially accumulates in our BR timecourse (Dataset S3), and all three sites are largely conserved in BES1 and its homologs (Fig S3). Thus, we mutated these three sites from serine to alanine (phosphorylation null) and tested BES1 phosphorylation status in *Nicotiana Benthamiana*. While more than half of the wild-type BES1-FLAG is phosphorylated one day after transfection, BES1[3SA]-FLAG exists mainly in dephosphorylated form (Fig S3). When co-expressed with BIN2, the phosphorylated form of wild-type BES1-FLAG was increased, while phosphorylated form of BES1[3SA]-FLAG was increased to a lesser extent, which supports the conclusion that S179, S180 and S171 are BIN2 phosphorylation sites (Fig S3).

In order to elucidate the functional consequences of the phosphorylation on S179, S180 and S171, we transformed *BES1-FLAG* and *BES1[3SA]-FLAG* to *bri1-301*, a weak allele of BR receptor BRI1 loss-of-function mutant, and assayed phosphorylation status in response to 100 nM BL. We found that BES1[3SA]-FLAG has lower levels of dephosphorylated BES1, and the amount of dephosphorylated BES1 increased more in response to BL treatment in BES1[3SA]-FLAG than in BES1-FLAG plants. Consistent with these observations, 18 out of 24 (75%) 3-week-old T1 plants overexpressing BES1[3SA]-FLAG showed stronger gain-of-function BR mutant phenotype, with elongated leaf petioles and curly leaves, compared to the 18 *bri1-301* plants overexpressing wild-type BES1-FLAG which did not show this phenotype (Fig S3). Further, it has been shown that the mutation of S173 in BZR1 (equivalent to S171 in BES1) alone did not change the phosphorylation status of BZR1 (12). Thus, these results support that BIN2

phosphorylates BES1 at S179, S180 and S171 to inhibit its function in BR-regulated signaling.

Downstream of kinase signaling, BES1 is predicted to regulate different downstream targets depending on whether its phosphosite levels (green, dashed) or transcript abundance (blue, solid) is used in the SC-ION pipeline. We mined Chromatin ImmunoPrecipitation (ChIP)-chip and ChIP-Seq datasets on BES1 and its homolog, BZR1 (40, 49, 64), and found that 88 out of 144 (61%) predicted first-neighbor targets of BES1, in our network, are directly bound by BES1 or its homolog BZR1 (Fig 3, orange circles; Table S1). Some of these validated genes with known roles in BR response include IAA3/SHORT HYPOCOTYL 2 (SHY2) (29), XYLOGLUCAN:XYLOGLUCOSYL TRANSFERASE 33 (XTH33) (49, 67) and SMALL AUXIN UP RNA 26 (SAUR26) (40). Thus, we were able to use our integrative omics network to identify previously unknown BIN2 phosphorylation sites on BES1 as well as validate its putative direct downstream targets identified by ChIP.

Network motif analysis predicts TFs involved in BR response. We next leveraged the network prediction to identify candidate genes involved in mediating the response to BR. We used the Network Motif Score (NMS) (7, 65) to classify genes in the TF-centered networks based on their presence in certain biological motifs, such as feedback and feed-forward loops. Genes with higher NMS scores have been shown to have a more important role in the biological process of interest (2, 7, 21, 34, 65). Accordingly, BES1 had the 25th highest NMS score (top 5%), illustrating that we could use the NMS to identify BR response regulators. We chose three TFs, ANTHOCYANLESS 2 (ANL2), TCX2, and BRON (AT1G75710), that had high (all in the top 35%) NMS scores in either the TF abundance or phosphosite GRNs (Dataset S5). We then examined subnetworks for each of these TFs, starting with kinase signaling and ending with transcriptional regulation.

SC-ION predicts that our first TF of interest, TCX2, and BES1/BZR1 HOMOLOG 2 (BEH2) regulate each other in a feedback loop (Fig S4A). Thus, we reasoned that TCX2 may regulate cell division in response to BR and treated the *tcx2-2* and *tcx2-3* mutants with 100 nM BL. In WT plants, the addition of BL causes a dramatic reduction in the root length. However, we did not find a significant difference in BL response in either of the *tcx2* mutant alleles compared to WT (Fig S4, Table S2).

We then focused on the subnetwork for ANL2, which predicts that ANL2 and BES1 regulate each other in a feedback loop (Fig S4). To test if ANL2 may be involved in BR response, we treated WT, *anl2-2*, and *anl2-3* plants with 100 nM BL. We found that *anl2* mutant roots shorten more than WT when treated with BL, demonstrating that the *anl2* mutants are hypersensitive to BL (Fig S4, Table S2). It has
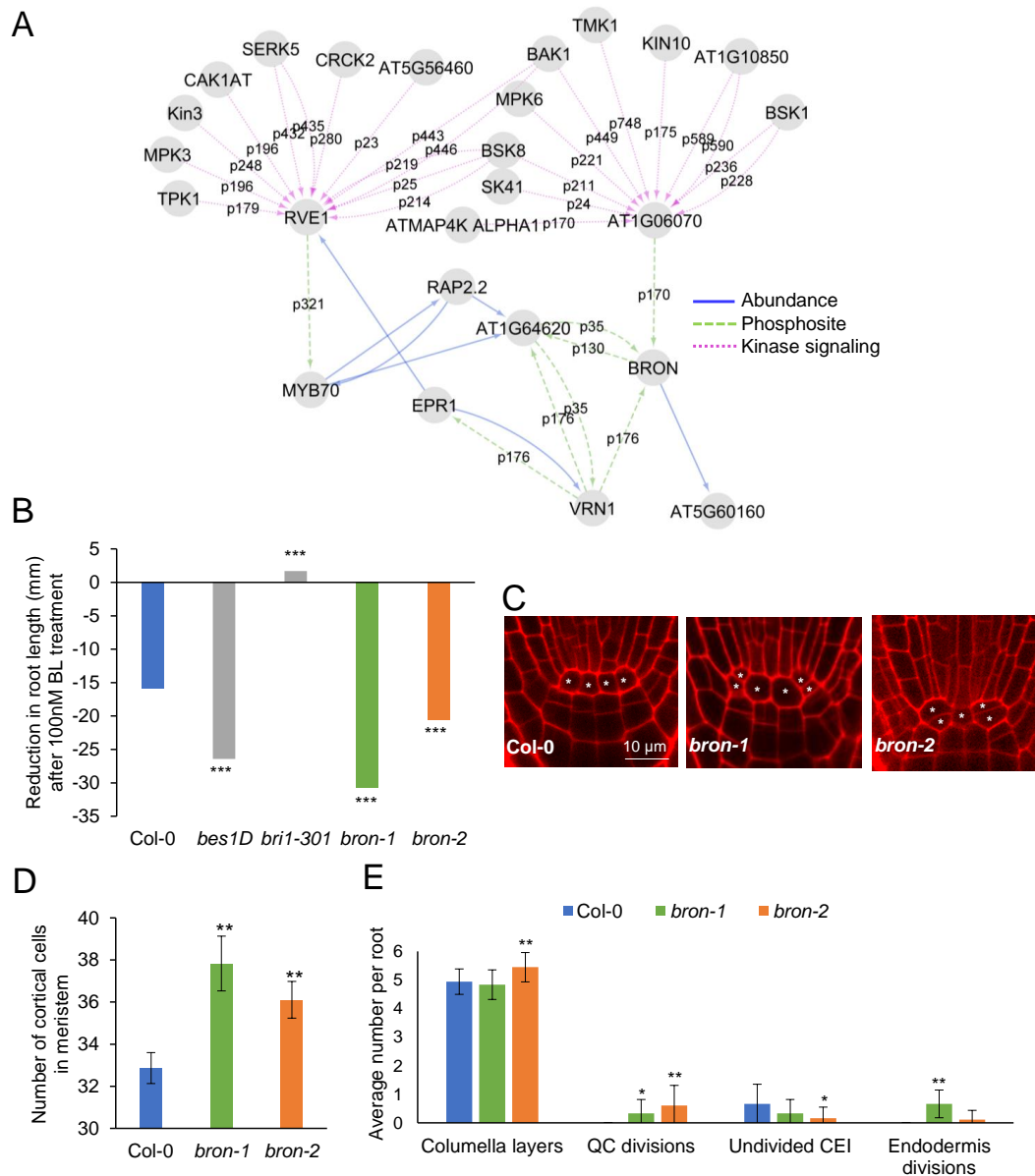
Fig. 4. *bron* mutant roots are hypersensitive to BL treatment and display excessive cell divisions. (A) BRON subnetwork. Edge labels represent the phosphosite used to predict that regulation. (B) *bron* mutants are hypersensitive to 100 nM BL treatment (n > 27). (C) Representative images of Col-0 wild type, *bron-1*, and *bron-2* root stem cell niches. * denote QC cells. (D) Number of meristematic cells in five-day old roots (n=18). (E) Average number of columella cell layers, QC divisions, undivided CEI, and endodermis division in five-day old roots (n=18). * denotes $p < 0.05$, ** $p < 0.01$, *** $p < 0.001$ using a generalized linear model (B) or Wilcoxon test (D&E).

also been shown that BL can induce excessive QC divisions in the root (14, 30, 53). Thus, we checked the *anl2* mutant roots for QC divisions as a secondary BR response phenotype: however, we found that *anl2* mutant roots do not display excessive QC divisions (Fig S4).

The TF BRONTOSAURUS (BRON) regulates cell division in response to BR. Our last TF of interest, BRON, is predicted to be regulated by TFs whose phosphorylation is dependent on multiple BR-signaling kinases such as BAK1, BSKs, and SERKs in our network (Fig 4A). We obtained a weak (*bron-1*) and a strong (*bron-2)* allele for BRON (Fig S5) and examined their BR response

as well as their root development (Fig 4B-E). We found that roots from both alleles shorten more in response to BL than wild type, demonstrating that *bron* mutant roots are hypersensitive to BL treatment (Fig 4B, Table S3). Additionally, we observed that *bron* mutants have longer roots with more meristematic cells (Fig S5), as well as significantly more divisions in the QC (Fig 4C-E). *bron-2* also displays excessive columella divisions and a higher number of undivided (i.e. actively dividing) CEI, while *bron-1* only shows excessive endodermis divisions, potentially due to its weaker effect on BRON expression (Fig 4E). This led us to hypothesize that BRON could regulate cell division in response to BR.

To determine the transcripts modulated by BRON, we performed RNA-seq on root tissue from the *bron-2* mutant (Dataset S7). We found that a range of BR-responsive genes were enriched in this mutant, particularly those genes repressed by BL after 15 minutes and induced by BL after 1 or 2 hours (p < 0.001) (Dataset S8). Further, we found that most of the genes have lower expression in the *bron-2* mutant, suggesting that BRON transcriptionally activates these genes (Fig S6).

Given the role of cyclins in regulating cell division (56), we specifically examined the expression of cyclins in the *bron-2* mutant. We found that four cyclins are differentially expressed in the *bron-2* mutant: three are repressed by BRON (*CYCD3;1, CYCP4;1, CYCP4;2*). Further, two of these cyclins, *CYCD3;1*, and *CYCP4;1*, are significantly induced by BL at 4 and 8 hours after treatment (Fig 5A). Importantly, it has been shown that *CYCD3;1* is induced by BL and contributes to BL-regulated cell division (14, 19). We also examined the cell-type-specific expression of *CYCD3;1*, *CYCP4;1*, and *BRON* in the root stem cells and mature root cells (7, 28), and we found key differences in where *CYCD3;1* and *CYCP4;1* are co-expressed with *BRON*. For example, *CYCP4;1* is co-expressed with *BRON* only in the QC. In contrast, *BRON* and *CYCD3;1* are co-expressed in the Epidermis/Lateral Root Cap (Epi/LRC) initials and the mature columella (Fig 5B). Taken together, these results suggest that BR incudes the expression of *CYCD3;1* and *CYCP4;1*, and therefore cell division, through the repression of BRON (Fig 5C).

Discussion

Here, we used a systems biology approach to unravel the temporal response to BR in *Arabidopsis*. By generating and integrating omics datasets, we were able to quantify how transcript, protein, and phosphorylation levels change in response to BR over time. We found that most of the (phospho)protein response occurs in the earlier timepoints (before 1 hour), whereas there are sets of early- and late-responsive transcripts (Fig 1). This suggested that BR first triggers the phosphorylation of TFs which then go on to regulate transcripts at later timepoints. Our predictive network reconstructed using SC-ION corroborated this hypothesis, illustrating how BR-responsive kinase signaling leads to phosphorylation of TFs and downstream transcriptional regulation (Fig 3). Further, our time-point specific networks allow us to predict which regulations occur early and late in BR response (Fig 2).

One well-known example of BR response involves the TFs BES1/BZR1, which are de-phosphorylated in response to BR, allowing them to move to the nucleus and transcriptionally regulate downstream genes. It is well-established that the GSK3 kinase BIN2 phosphorylates BES1/BZR1 to negatively regulate their functions through the promotion

of the cytoplasmic retention, inhibition of DNA binding and protein degradation of BES1/BZR1 (39). Although there are more than 20 predicted sites, the exact BIN2 phosphorylation sites on BES1 are not functionally characterized. Through our omics profiling and network analysis, we predicted that S171, S179 and S180 in BES1 are potentially phosphorylated by BIN2. Further mutational analysis indicated that the phosphorylation of the three sites contributed to BES1 phosphorylation by BIN2 and are important for BES1 activity. In contrast, the mutation of S173 in BZR1 (equivalent to S171 in BES1) affected BZR1 interaction with 14-3-3 and nuclear localization but did not change its phosphorylation status (12). Our study therefore identified three key BIN2 phosphorylation sites that negatively regulate BES1 activity and hence BR signaling (Fig S3).

We further used our network to predict novel roles for the TFs ANL2 and BRON in BR response (Figs 4 and 5, Fig S4). We found that mutants of both TFs are hypersensitive to BL treatment, but only *bron* mutants display excessive cell divisions. Given *anl2*'s hypersensitivity to BL, it would be interesting to investigate its role in BR response in the future, given that it likely has a different role than BRON. We additionally found a significant overlap between genes differentially expressed in the *bron-2* mutant and genes induced or repressed by BR. Specifically, we observed a significant overlap in disease resistance, drought response, and stress response genes which were repressed by BL 15 minutes after treatment and repressed in the *bron-2* mutant (Fig S6). Crosstalk between BR and drought response is well known and involves other TFs such as WRKY46/54/70, RD26 and TINY (6, 38, 59, 61), but the temporal aspects of this signaling have not been previously examined. Our observation that BRON is regulated by BLs as early as 15 minutes after treatment suggests that inhibition of stress responses quickly follows activation of the BR pathway.

We found that cyclin genes, specifically *CYCD3;1* and *CYCP4;1*, are induced by BL and repressed by BRON, suggesting that BR induces these cyclins through its repression of BRON (Fig 5C). These results are supported by multiple studies which elucidate the role of CYCD3;1 in BR-induced cell division (14, 19) and describe how BR specifically induces QC division in the root (14, 30, 53). While *CYCP4;1* has not been directly implicated in BR response, its co-expression with *CYCD3;1* in both the bron mutant and BL time course suggests that it may have a similar function as CYCD3;1 in the Arabidopsis root. Further, by mining cell-type-specific transcriptomic datasets (7, 28), we gained insight into the cell types in which these cyclins are active. We found that *CYCP4;1* and *BRON* are specifically co-expressed in the QC, suggesting that BRON may repress QC division through CYCP4;1. In contrast, *CYCD3;1* and *BRON* are co-expressed in the Epi/LRC stem cell initials as well as the
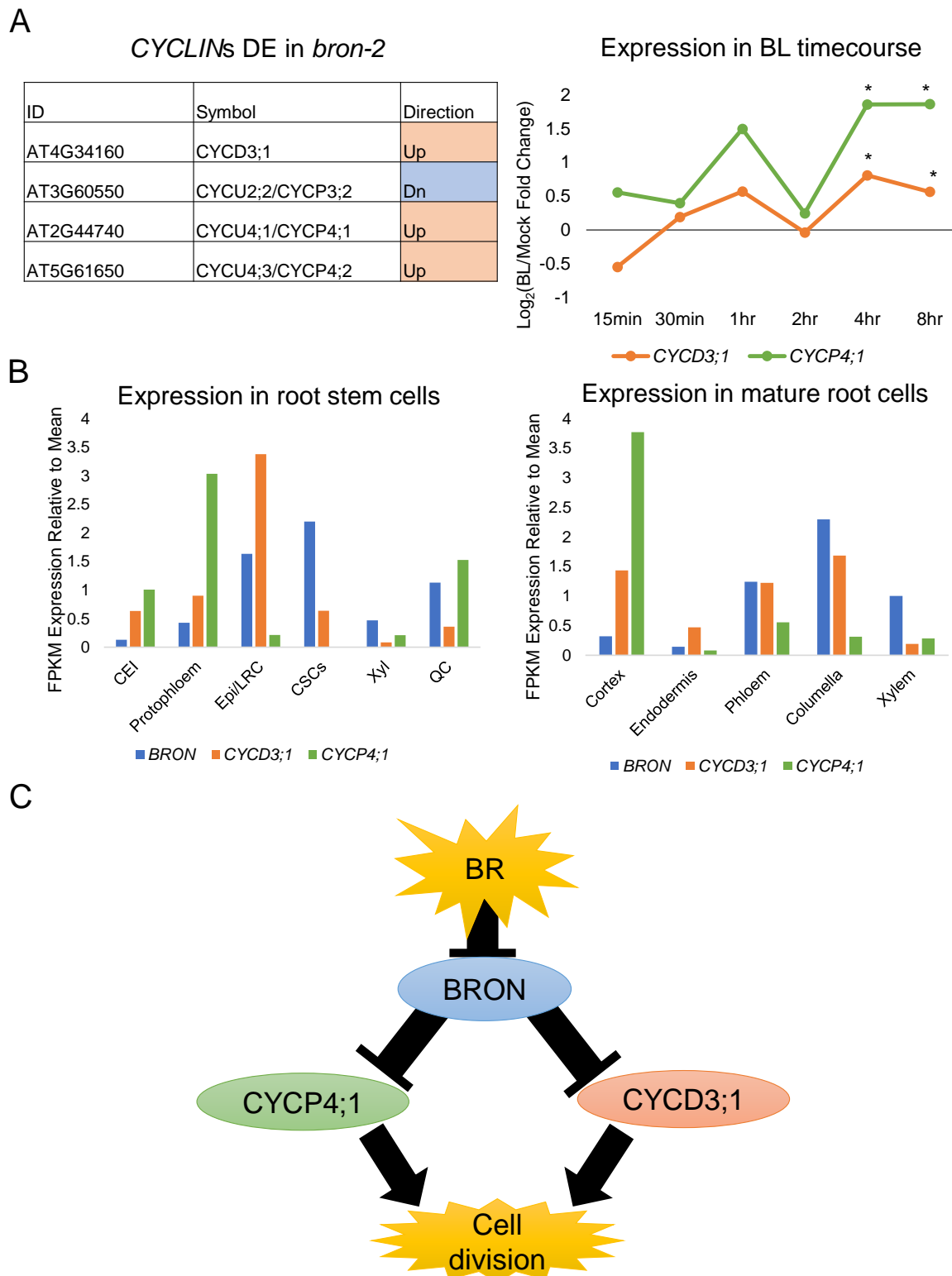
Fig. 5. BRON regulates cell division in response to BR through inhibiting cyclins. (A) (left) Cyclins differentially expressed in the bron-2 mutant. (right) BL/Mock transcript fold change of *CYCD3;1* (orange) and *CYCP4;1* (green) in the BL time course. * denotes the gene is differentially expressed in response to BL at that time point. (B) Transcript expression of *BRON* (blue), *CYCD3;1* (orange), and *CYCP4;1* (green) in root stem cell populations (left) and mature root tissues (right). CEI – Cortex Endodermis Initials; Epi/LRC – Epidermis/Lateral Root Cap initials; CSCs – Columella Stem Cells; Xyl – Xylem initials; QC- Quiescent Center. (C) Proposed model for the role of BRON in BR response. BR represses BRON, which represses the cyclins *CYCD3;1* and *CYCP4;1*. This leads to BR-induced cell division.

mature columella. We found that *bron-2* mutants have excessive columella divisions (Fig 4E), suggesting that perhaps BRON represses cell division in the columella and lateral root cap through CYCD3;1. It would be of interest in the future to unravel BRON's cell-type-specific repression of cell division in response to BR.

Taken together, our temporal, integrated omics dataset, kinase-signaling and TF-centered networks can be used as a resource to identify additional genes like BRON which are implicated in BR response in *Arabidopsis*.

Methods

Plant Materials and Growth Conditions. The Arabidopsis accession Columbia-0 was used as the wild type control in all experiments. The T-DNA insertion mutants *tcx2-2* (SAIL_808_H08), *tcx2-3* (SALK_021952), *anl2-2* (SALK_000196C), and *anl2-3* (SAIL_418_C10) were described previously (7). The *bes1-D* and *bri1-301* mutants were also described previously (11, 53, 60, 63). The T-DNA insertion mutants *at1g75710/bron-1* (SALK_048268) and *at1g75710/bron-2* (SALK_046220C) were obtained from the Arabidopsis Biological Resource Center (ABRC: https://abrc.osu.edu/).

For the BL time series profiling experiments, WT seeds were sterilized with 70% EtOH + 0.1% Triton for 15 minutes, washed with 100% EtOH 3 times and plated on 1/2 LS plates with 1% sucrose and 1000 nM BRZ with nylon mesh overlaid on top of the agar. After 3 days of stratification at 4°C, the plates were placed under continuous light at 22°C for 7 days. BL treatments were performed by transferring the seedlings on the nylon mesh to 1/2 LS liquid medium with either 1 μM BL or DMSO for 15 min, 30 min, 1 hr, 2 hr, 4 hr, or 8 hr. Four biological replicates were collected for BL- and mock-treated samples at each time point (48 samples total). Samples were blotted dry with Kimwipes, flash frozen in liquid nitrogen, and ground for 15 minutes under liquid nitrogen using a mortar and pestle.

For the *bron-2* RNA-seq experiment, seeds were wet sterilized using 50% bleach, 10% Tween and water and stratified at 4°C for 2 days. Seeds were plated on 1x MS, 1% sucrose plates with Nitex mesh and grown under long day conditions (16 hr light/8 hr dark) at 22°C for 5 days. Three biological replicates of 10 plates each were collected.

BES1 Western Blot. To monitor BES1 protein levels and phosphorylation status, BL treatment was performed as described above. Approximately 100 mg of ground tissue powder was resuspended directly in 300 μL 2xSDS sample buffer (100 mM Tris-Cl, pH 6.8, 4% (w/v) sodium dodecyl sulfate, 0.2% (w/v) bromophenol blue, 20% (v/v) glycerol and 200 mM dithiothreitol) before SDS-PAGE and western blotting using anti-BES1 antibody (64).

RNA Sequencing and Data Analysis. For the BR time-course, total RNA was extracted using Zymo Direct-zol kit (Zymo Research). RNA concentration was measured with Qubit RNA HS assays (ThermoFisher #Q10213) and integrity checked with AATI Fragment Analyzer with Standard Sensitivity RNA Analysis Kit (DNF-489-0500). Approximately 500 ng of RNA was used for library construction via the QuantSeq 3' mRNA-Seq Library Prep FWD Kit for Illumina. Sequencing was performed on a HiSeq 3000 with 50 bp single end reads. Raw sequencing data are deposited at the Gene Expression Omnibus (https://www.ncbi.nlm.nih.gov/geo/query/acc.cgi?acc=GSE147589, accession token ibmjqk-wczvwdvwn). Reads were mapped to the TAIR10 genome using the STAR aligner (10). Differential expression was performed using PoissonSeq (27) using a *q*-value cutoff of 0.05 and a fold-change cutoff of 1.25.

For *bron-2* transcriptional profiling, total RNA was isolated from approximately 2 mm of five-day-old Col-0 and *bron-2* root tips using the RNeasy Micro Kit. cDNA synthesis and amplification were performed using the NEBNext Ultra II RNA Library Prep Kit for Illumina. Libraries were sequenced on an Illumina HiSeq 2500 with 100 bp single-end reads. Reads were mapped to the TAIR10 genome using Cufflinks (51). Differential expression was performed using PoissonSeq with a *p*-value cutoff of 0.05. Raw sequencing data are deposited at the Gene Expression Omnibus (https://www.ncbi.nlm.nih.gov/geo/query/acc.cgi?acc=GSE157000, accession token ivabyi-uypzwxvil).

Protein Extraction and Digestion. The proteomics experiments were carried out based on established methods (46–48). Protein was extracted from aliquots of the tissue used for transcriptome profiling and digested into peptides with trypsin and Lys-C using the phenol-FASP method detailed in (46, 48). Resulting peptides were desalted using 50 mg Sep-Pak C18 cartridges (Waters), dried using a vacuum centrifuge (Thermo), and resuspended in 0.1% formic acid. Peptide amount was quantified using the Pierce BCA Protein assay kit.

Tandem Mass Tag (TMT) Labeling. The TMT labeling strategy used in this experiment is provided in Table S3. 45 μg of peptides were taken from each individual sample, pooled, and then split into two pooled references. TMT10plex™ label reagents (ThermoFisher, Lot UD280154) were used to label 200 μg of peptides, from each sample or pooled reference, at a TMT:peptide ratio of 0.2:1 as described in (48). After 2 hours incubation at room temperature the labeling reaction was quenched with hydroxylamine. Next, the ten samples were mixed together, an aliquot of 75μg of peptides was reserved for protein abundance profiling, and the remaining peptides were used for phosphopeptide enrichment and stored at -80ºC.

Phosphopeptide Enrichment. The TMT-labeled phosphopeptides were first enriched using the High-Select TiO_2 Phosphopeptide Enrichment Kit (Thermo) using the manufacturers protocol. The High-Select Fe-NTA Phosphopeptide Enrichment Kit (Thermo) was then used on the flowthrough from the TiO_2 enrichment to enrich additional phosphopeptides. The manufacturers protocol for the Fe-NTA kit was used except the final eluate was re-suspended with 50 μL 0.1% formic acid. The eluates from the TiO_2 and Fe-NTA enrichments were combined and stored at -80ºC until analysis by LC/MS-MS.

LC/MS-MS. An Agilent 1260 quaternary HPLC was used to deliver a flow rate of 600 nL min-1 via a splitter. All columns were packed in house using a Next Advance pressure cell, and the nanospray tips were fabricated using a fused silica capillary that was pulled to a sharp tip using a laser puller (Sutter P-2000). 25 μg of TMT-labeled peptides (non-modified proteome), or 10 μg TiO_2 enriched peptides (phosphoproteome), were loaded onto 20 cm capillary columns packed with 5 μM Zorbax SB-C18 (Agilent), which was connected using a zero dead volume 1 μm filter (Upchurch, M548) to a 5 cm long strong cation exchange (SCX) column packed with 5 μm PolySulfoethyl (PolyLC). The SCX column was then connected to a 20 cm nanospray tip packed with 2.5 μM C18 (Waters). The 3 sections were joined and mounted on a Nanospray Flex ion source (Thermo) for on-line nested peptide elution. A new set of columns was used for every sample. Peptides were eluted from the loading column onto the SCX column using a 0 to 80% acetonitrile gradient over 60 minutes. Peptides were then fractionated from the SCX column using a series of 18 and 6 salt steps (ammonium acetate) for the non-modified proteome and phosphoproteome analysis, respectively. For these analyses, buffers A (99.9% H2O, 0.% formic acid), B (99.9% ACN, 0.1% formic acid), C (100 mM ammonium acetate, 2% formic acid), and D (2 M ammonium acetate, 2% formic acid) were utilized. For each salt step, a 150-minute gradient program comprised of a 0–5 minute increase to the specified ammonium acetate concentration, 5–10 minutes hold, 10–14 minutes at 100% buffer A, 15–120 minutes 10–35% buffer B, 120–140 minutes 35–80% buffer B, 140–145 minutes 80% buffer B, and 145–150 minutes buffer A was employed.

Eluted peptides were analyzed using a Thermo Scientific Q-Exactive Plus high-resolution quadrupole Orbitrap mass spectrometer, which was directly coupled to the HPLC. Data dependent acquisition was obtained using Xcalibur 4.0 software in positive ion mode with a spray voltage of 2.10 kV and a capillary temperature of 275 °C and an RF of 60. MS1 spectra were measured at a resolution of 70,000, an automatic gain control (AGC) of 3e6 with a maximum ion time of 100 ms and a mass range of 400-2000 m/z. Up to 15 MS2 were triggered at a resolution of 35,000 with a fixed first mass of 120 m/z for phosphoproteome and 115

m/z for proteome. An AGC of 1e5 with a maximum ion time of 50 ms, an isolation window of 1.3 m/z, and a normalized collision energy of 33. Charge exclusion was set to unassigned, 1, 5–8, and >8. MS1 that triggered MS2 scans were dynamically excluded for 45 or 25 s for phospho- and non-modified proteomes, respectively.

Proteomics Data Analysis. The raw data were analyzed using MaxQuant version 1.6.3.3 (52). Spectra were searched, using the Andromeda search engine in MaxQuant (9) against the Tair10 proteome file entitled "TAIR10_pep_20101214" that was downloaded from the TAIR website (https://www.arabidopsis.org/download_files/Proteins/ TAIR10_protein_lists/TAIR10_pep_20101214) and was complemented with reverse decoy sequences and common contaminants by MaxQuant. Carbamidomethyl cysteine was set as a fixed modification while methionine oxidation and protein N-terminal acetylation were set as variable modifications. For the phosphoproteome "Phospho STY" was also set as a variable modification. The sample type was set to "Reporter Ion MS2" with "10plex TMT selected for both lysine and N-termini". TMT batch-specific correction factors were configured in the MaxQuant modifications tab (TMT Lot UD280154). Digestion parameters were set to "specific" and "Trypsin/P;LysC". Up to two missed cleavages were allowed. A false discovery rate, calculated in MaxQuant using a target-decoy strategy (Elias and Gygi, 2007), less than 0.01 at both the peptide spectral match and protein identification level was required. The 'second peptide' option identify co-fragmented peptides was not used. The match between runs feature of MaxQuant was not utilized. Raw proteomics data have been deposited on MassIVE and can be accessed at the link ftp://MSV000085606@massive.ucsd.edu with reviewer username "MSV000085606_reviewer" and password "Clark_BL".

Statistical analysis was performed using TMT-NEAT Analysis Pipeline version 1.3 (https://github.com/nmclark2/TMT-Analysis-Pipeline). This pipeline takes the "proteinGroups" (protein abundance) or "Phospho(STY)Sites" (phosphoproteome) tables output from MaxQuant as well as a metadata file detailing the TMT labeling scheme and sample information as input. Example input files are provided in the GitHub repository. First, the MaxQuant output table is trimmed to only include the needed information for statistical analysis, and the columns are re-labeled using the provided sample information. Contaminants are removed at this stage. Next, data are normalized using the sample loading normalization and internal reference normalization methods such that samples can be compared across runs (42). Quantitative plots such as boxplots, hierarchical clustering, and principal components analysis are provided for quality control. Finally, statistical analysis is performed using PoissonSeq (27) and histograms of p- or q-value dis-

tributions are generated. Proteins and phosphosites were categorized as differentially accumulating if they had a *p*-value < 0.05 and fold-change > 1.1.

GO Analyses. GO analysis on the DE transcripts, protein, and phosphoproteins was performed using PANTHER (33). Genes were separated depending on whether they were induced or repressed by BL in early (1 hr or prior) or late (after 1 hr) time points. Biological process GO terms were considered significantly enriched if they had a corrected p-value 0.05 (Dataset S4).

Gene Regulatory Network Inference. TF-centered gene regulatory networks were inferred using SC-ION version 2.0 (https://github.com/nmclark2/SCION). SC-ION builds on the RTP-STAR pipeline (7, 65) by incorporating DTW and ICA clustering (13, 37) and integration of different data types. SC-ION uses an adapted version of GENIE3 (20) which allows for separate regulator and target data matrices (54). This allows the user, for example, to use protein abundance data for regulators (TFs) and transcript data for targets (all genes). SC-ION takes regulator and target lists and regulator and target data matrices as input. In addition, SC-ION takes a clustering data matrix which can be different from the regulator and target data matrices. This allows the user to cluster genes based on different datatypes. A version of SC-ION without this clustering step is also available. SC-ION outputs a table of the predicted regulations as well as a weight for each edge, where a higher weight indicates higher confidence in that inferred edge (20). This table can be imported into software such as Cytoscape (45) for network visualization. Test input files for SC-ION are provided on GitHub.

Two TF-centered networks were inferred. In the first network, TF protein abundance (when quantified) or TF transcript abundance (when cognate protein was not quantified) was used as the "regulator" value to infer their "target" genes' transcript abundance. In the second phosphosite network, we inferred the transcript levels of "target" genes using TF phosphosite intensities as "regulators." In both networks, the clustering matrix was constructed by combining the "regulator" (TF abundance) and "target" (transcript levels) data so that genes were clustered based on the protein/phosphosite levels of the regulators and transcript levels of the targets. Clustering was then performed using the DTW method given the temporal nature of our data. Six sub-networks were inferred for each TF-centered network, where each sub-network represents the regulations predicted to happen using only one time point (15 min, 30 min, 1 hr, 2 hr, 4 hr, 8 hr). To achieve this, only the genes DE at each time point were used in these individual subnetworks. This allows us to denote which regulations are predicted to happen early or late in BR response. The six subnetworks were merged in Cytoscape to form the final abundance and phosphosite networks. Cytoscape was also used to create the merged abundance, phosphosite, and kinase signaling networks

(Dataset S5).

We have previously used the Normalized Motif Score (NMS) to predict biologically important genes in GRNs from Arabidopsis (7, 65). Four different motifs were used to calculate the NMS for the merged abundance and phosphosite networks separately: feed-forward loops, feedback loops, diamond motifs, and bi-fan motifs. First, the number of times a gene appeared in each motif was counted using the NetMatchStar app (43) in Cytoscape. Then, the counts were normalized to a scale from 0 to 1 and summed to calculate the NMS for each gene.

Activation loop domains, also called p-loop domains, in protein kinases were identified using a modified version of the pipeline described in (55). Briefly, all 35,386 protein sequences available in the TAIR10 annotation were searched for kinase domains using The National Center for Biotechnology Information batch conserved domain search tool (31). From this list of 1,522 proteins with identified kinase domains, 878 were also annotated with activation loop (p-loop) coordinates by the search tool. The kinase domains of proteins lacking the p-loop coordinates were aligned using MAFFT (22). The resulting alignment was manually searched for the well conserved p-loop beginning (DFG) and end (APE) motifs. An extra 482 p-loop coordinates were obtained, for a total of 1,360 protein kinases with p-loop coordinates.

The kinase signaling regulatory network was inferred using a previously described correlation-based approach (55). Kinases with phosphosites in the p-loop domain that were DE in response to BL were used as the potential regulators. All genes with phosphosites that were DE in response to BL were used as the potential targets. We used phosphosite intensity rather than abundance for the regulators as it has been shown that phosphosite intensity has greater predictive power (55) (Fig S2). Pearson and Spearman correlations were calculated for each regulator-target pair, and edges were kept for those pairs with Pearson correlation 0.5 or Spearman correlation 0.6.

Mutant BES1 Cloning and Protein Level Detection. The three Serine to Alanine mutations were introduced by two-step PCR using the primers provided in Table S4. Two BES1 fragments were generated and combined to form the full-length mutant BES1. The full-length mutant BES1 was then cloned to *Pro35S:FLAG* vector to generate *Pro35S:BES1^{S3A}-FLAG*. *Pro35S:BES1-FLAG* was subcloned from *Pro35S:BES1-GFP* (63).

For transient expression in *Nicotiana benthamiana*, agrobacterium containing *Pro35S:BES1-FLAG* or *Pro35S:BES1^{S3A}-FLAG* was infiltrated to mature *N. benthamiana* leaves. Agrobacterium containing *Pro35S:YFP-BIN2* was used for co-expression. Leaf discs were collected 24 hours after infiltration and flash frozen in

liquid nitrogen. The samples were ground in 2xSDS buffer and resolved on SDS-PAGE. Anti-Flag antibody was used for western blotting.

To test BES1 phosphorylation status in response to BR, T1 seeds from transgenic plants overexpressing *Pro35S:BES1-FLAG* or *Pro35S:BES1^{S3A}-FLAG* were germinated on 1/2MS plates containing 1uM BRZ and 50mg/ml Kanamycin. Ten-day-old seedlings were collected and subjected to 100nM BL treatment. DMSO was used as control. Twelve seedlings were used for each treatment. The samples were ground in 2xSDS buffer and resolved on SDS-PAGE. Anti-Flag antibody was used for western blotting.

BR Phenotyping Methods. BL phenotyping were carried out as previously described (58). Seeds were sterilized for 4 hours in a Nalgene Acrylic Desiccator Cabinet (Fisher Scientific, 08-642-22) by mixing 200mL bleach (8.25% sodium hypochlorite) with 8mL concentrated hydrochloric acid to generate chlorine gas. Seeds were then resuspended using 0.1% agarose solution for plating. Control (BL0; DMSO solvent only) or BL100 treated (100nM Brassinolide; BL, Wako chemicals) were plated on ½ LS plates supplemented with 1% (w/v) sucrose. After seeds were plated, the plates were sealed with breathable tape (3M Micropore) and placed in the dark at 4°C for 5 days for stratification. Plants were grown for 7 days at 22°C under continuous light. Plates were imaged with an Epson Perfection V600 Flatbed Photo scanner at a resolution of 1200 DPI and root length was then measured in ImageJ.

***bron* Mutant Genotyping and Root Phenotyping.** RT-qPCR was performed on *bron-1* and *bron-2* mutant alleles as described in (7) to measure *BRON* expression. Total RNA was isolated from approximately 2mm of five-day-old Col-0, *bron-1* and *bron-2* root tips using the RNeasy Micro Kit (Qiagen). qPCR was performed with SYBR green (Invitrogen) using a 7500 Fast Real-Time PCR system (Applied Biosystems) with 40 cycles. Data were analyzed using the Ct (cycle threshold) method and normalized to the expression of the reference gene UBIQUITIN10 (UBQ10). qPCR was performed on two technical replicates of three independent RNA samples (biological replicates). Primers used for qPCR are provided in Table S4.

Confocal imaging was performed on a Zeiss LSM 710. Cell walls were counterstained using propidium iodide (PI). The number of meristematic cells and cell divisions were manually counted.

Statistics. A generalized mixed linear model with penalized quasi-likelihood (glmmPQL in R) was used to determine the genotype x treatment interaction *p*-values for the BL phenotyping experiment. In this model, the genotype and treatment effects were considered fixed,

and the experiment date and plate number were considered random effects with a Gaussian error distribution. Hypergeometric and/or Chi-squared tests were used for test for enrichment in the RNAseq DE gene lists. For *bron* mutant root phenotyping, a two-tailed Wilcoxon test was used for statistical significance as some of the data did not follow a normal distribution. To select *p*- and *q*- value cutoffs for the large-scale omics experiments, we used the distribution of *p*- and *q*- values generated from the statistical tests as described in (5, 8).

References

1. ADAMS, J. A. Activation loop phosphorylation and catalysis in protein kinases: is there functional evidence for the autoinhibitor model? *Biochemistry 42*, 3 (Jan. 2003), 601–607.

2. ALON, U. Network motifs: theory and experimental approaches. *Nature Reviews Genetics 8*, 6 (June 2007), 450–461. Number: 6 Publisher: Nature Publishing Group.

3. ASAMI, T., MIN, Y. K., NAGATA, N., YAMAGISHI, K., TAKATSUTO, S., FUJIOKA, S., MUROFUSHI, N., YAMAGUCHI, I., AND YOSHIDA, S. Characterization of Brassinazole, a Triazole-Type Brassinosteroid Biosynthesis Inhibitor. *Plant Physiology 123*, 1 (May 2000), 93–100. Publisher: American Society of Plant Biologists Section: DEVELOPMENT AND HORMONE ACTION.

4. BEEKHOF, R., VAN ALPHEN, C., HENNEMAN, A. A., KNOL, J. C., PHAM, T. V., ROLFS, F., LABOTS, M., HENNEBERRY, E., LE LARGE, T. Y., DE HAAS, R. R., PIERSMA, S. R., VURCHIO, V., BERTOTTI, A., TRUSOLINO, L., VERHEUL, H. M., AND JIMENEZ, C. R. INKA, an integrative data analysis pipeline for phosphoproteomic inference of active kinases. *Molecular Systems Biology 15*, 4 (Apr. 2019), e8250. Publisher: John Wiley & Sons, Ltd.

5. BREHENY, P., STROMBERG, A., AND LAMBERT, J. p-Value Histograms: Inference and Diagnostics. *High-Throughput 7*, 3 (Aug. 2018).

6. CHEN, J., NOLAN, T. M., YE, H., ZHANG, M., TONG, H., XIN, P., CHU, J., CHU, C., LI, Z., AND YIN, Y. Arabidopsis WRKY46, WRKY54, and WRKY70 Transcription Factors Are Involved in Brassinosteroid-Regulated Plant Growth and Drought Responses. *The Plant Cell 29*, 6 (June 2017), 1425–1439. Publisher: American Society of Plant Biologists Section: Research Article.

7. CLARK, N. M., BUCKNER, E., FISHER, A. P., NELSON, E. C., NGUYEN, T. T., SIMMONS, A. R., DE LUIS BALAGUER, M. A., BUTLER-SMITH, T., SHELDON, P. J., BERGMANN, D. C., WILLIAMS, C. M., AND SOZZANI, R. Stem-cell-ubiquitous genes spatiotemporally coordinate division through regulation of stem-cell-specific gene networks. *Nature Communications 10*, 1 (Dec. 2019), 5574. Number: 1 Publisher: Nature Publishing Group.

8. CLARK, N. M., SHEN, Z., BRIGGS, S. P., WALLEY, J. W., AND KELLEY, D. R. Auxin Induces Widespread Proteome Remodeling in Arabidopsis Seedlings. *PROTEOMICS 19*, 17 (2019), 1900199. _eprint: https://onlinelibrary.wiley.com/doi/pdf/10.1002/pmic.201900199.

9. COX, J., NEUHAUSER, N., MICHALSKI, A., SCHELTEMA, R. A., OLSEN, J. V., AND MANN, M. Andromeda: A Peptide Search Engine Integrated into the MaxQuant Environment. *Journal of Proteome Research 10*, 4 (Apr. 2011), 1794–1805. Publisher: American Chemical Society.

10. DOBIN, A., DAVIS, C. A., SCHLESINGER, F., DRENKOW, J., ZALESKI, C., JHA, S., BATUT, P., CHAISSON, M., AND GINGERAS, T. R. STAR: ultrafast universal RNA-seq aligner. *Bioinformatics 29*, 1 (Jan. 2013), 15–21. Publisher: Oxford Academic.

11. FRIEDRICHSEN, D. M., JOAZEIRO, C. A. P., LI, J., HUNTER, T., AND CHORY, J. Brassinosteroid-Insensitive-1 Is a Ubiquitously Expressed Leucine-Rich Repeat Receptor Serine/Threonine Kinase. *Plant Physiology 123*, 4 (Aug. 2000), 1247–1256. Publisher: American Society of Plant Biologists Section: DEVELOPMENT AND HORMONE ACTION.

12. GAMPALA, S. S., KIM, T.-W., HE, J.-X., TANG, W., DENG, Z., BAI, M.-Y., GUAN, S., LALONDE, S., SUN, Y., GENDRON, J. M., CHEN, H., SHIBAGAKI, N., FERL, R. J., EHRHARDT, D., CHONG, K., BURLINGAME, A. L., AND WANG, Z.-Y. An Essential Role for 14-3-3 Proteins in Brassinosteroid Signal Transduction in Arabidopsis. *Developmental Cell 13*, 2 (Aug. 2007), 177–189.

13. GIORGINO, T. Computing and Visualizing Dynamic Time Warping Alignments in *R* : The **dtw** Package. *Journal of Statistical Software 31*, 7 (2009).

14. GONZÁLEZ-GARCÍA, M.-P., VILARRASA-BLASI, J., ZHIPONOVA, M., DIVOL, F., MORA-GARCÍA, S., RUSSINOVA, E., AND CAÑO-DELGADO, A. I. Brassinosteroids control meristem size by promoting cell cycle progression in Arabidopsis roots. *Development 138*, 5 (Mar. 2011), 849–859. Publisher: Oxford University Press for The Company of Biologists Limited Section: DEVELOPMENT AND STEM CELLS.

15. HE, J.-X., GENDRON, J. M., SUN, Y., GAMPALA, S. S. L., GENDRON, N., SUN, C. Q., AND WANG, Z.-Y. BZR1 Is a Transcriptional Repressor with Dual Roles in Brassinosteroid Homeostasis and Growth Responses. *Science 307*, 5715 (Mar. 2005), 1634–1638. Publisher: American Association for the Advancement of Science Section: Report.

16. HE, J.-X., GENDRON, J. M., YANG, Y., LI, J., AND WANG, Z.-Y. The GSK3-like kinase BIN2 phosphorylates and destabilizes BZR1, a positive regulator of the brassinosteroid signaling pathway in Arabidopsis. *Proceedings of the National Academy of Sciences 99*, 15 (July 2002), 10185–10190. Publisher: National Academy of Sciences Section: Biological Sciences.

17. HE, Z., WANG, Z.-Y., LI, J., ZHU, Q., LAMB, C., RONALD, P., AND CHORY, J. Perception of Brassinosteroids by the Extracellular Domain of the Receptor Kinase BRI1. *Science 288*, 5475 (June 2000), 2360–2363. Publisher: American Association for the Advancement of Science Section: Report.

18. HOGREBE, A., VON STECHOW, L., BEKKER-JENSEN, D. B., WEINERT, B. T., KELSTRUP, C. D., AND OLSEN, J. V. Benchmarking common quantification strategies for large-scale phosphoproteomics. *Nature Communications 9*, 1 (Dec. 2018), 1045. Publisher: Nature Publishing Group.

19. HU, Y., BAO, F., AND LI, J. Promotive effect of brassinosteroids on cell division involves a distinct CycD3-induction pathway in Arabidopsis. *The Plant Journal 24*, 5 (2000), 693–701. _eprint: https://onlinelibrary.wiley.com/doi/pdf/10.1046/j.1365-313x.2000.00915.x.

20. HUYNH-THU, V. A., IRRTHUM, A., WEHENKEL, L., AND GEURTS, P. Inferring Regulatory Networks from Expression Data Using Tree-Based Methods. *PLOS ONE 5*, 9 (Sept. 2010), e12776. Publisher: Public Library of Science.

21. INGRAM, P. J., STUMPF, M. P., AND STARK, J. Network motifs: structure does not determine function. *BMC Genomics 7*, 1 (May 2006), 108.

22. KATOH, K., AND STANDLEY, D. M. MAFFT Multiple Sequence Alignment Software Version 7: Improvements in Performance and Usability. *Molecular Biology and Evolution 30*, 4 (Apr. 2013), 772–780. Publisher: Oxford Academic.

23. KIM, E.-J., AND RUSSINOVA, E. Brassinosteroid signalling. *Current Biology 30*, 7 (Apr. 2020), R294–R298. Publisher: Elsevier.

24. LI, J., AND CHORY, J. A Putative Leucine-Rich Repeat Receptor Kinase Involved in Brassinosteroid Signal Transduction. *Cell 90*, 5 (Sept. 1997), 929–938.

25. LI, J., NAM, K. H., VAFEADOS, D., AND CHORY, J. BIN2, a New Brassinosteroid-Insensitive Locus in Arabidopsis. *Plant Physiology 127*, 1 (Sept. 2001), 14–22. Publisher: American Society of Plant Biologists Section: DEVELOPMENT AND HORMONE ACTION.

26. LI, J., WEN, J., LEASE, K. A., DOKE, J. T., TAX, F. E., AND WALKER, J. C. BAK1, an Arabidopsis LRR Receptor-like Protein Kinase, Interacts with BRI1 and Modulates Brassinosteroid Signaling. *Cell 110*, 2 (July 2002), 213–222.

27. LI, J., WITTEN, D. M., JOHNSTONE, I. M., AND TIBSHIRANI, R. Normalization, testing, and false discovery rate estimation for RNA-sequencing data. *Biostatistics 13*, 3 (July 2012), 523–538. Publisher: Oxford Academic.

28. LI, S., YAMADA, M., HAN, X., OHLER, U., AND BENFEY, P. High-Resolution Expression Map of the Arabidopsis Root Reveals Alternative Splicing and lincRNA Regulation. *Developmental Cell 39*, 4 (Nov. 2016), 508–522.

29. LI, T., KANG, X., LEI, W., YAO, X., ZOU, L., ZHANG, D., AND LIN, H. SHY2 as a node in the regulation of root meristem development by auxin, brassinosteroids, and cytokinin. *Journal of Integrative Plant Biology n/a*, n/a (2020). _eprint: https://onlinelibrary.wiley.com/doi/pdf/10.1111/jipb.12931.

30. LOZANO-ELENA, F., PLANAS-RIVEROLA, A., VILARRASA-BLASI, J.,

SCHWAB, R., AND CAÑO-DELGADO, A. I. Paracrine brassinosteroid signaling at the stem cell niche controls cellular regeneration. *Journal of Cell Science 131*, 2 (Jan. 2018). Publisher: The Company of Biologists Ltd Section: Research Article.

31. LU, S., WANG, J., CHITSAZ, F., DERBYSHIRE, M. K., GEER, R. C., GONZALES, N. R., GWADZ, M., HURWITZ, D. I., MARCHLER, G. H., SONG, J. S., THANKI, N., YAMASHITA, R. A., YANG, M., ZHANG, D., ZHENG, C., LANCZYCKI, C. J., AND MARCHLER-BAUER, A. CDD/SPARCLE: the conserved domain database in 2020. *Nucleic Acids Research 48*, D1 (Jan. 2020), D265–D268. Publisher: Oxford Academic.

32. MCALISTER, G. C., HUTTLIN, E. L., HAAS, W., TING, L., JEDRYCHOWSKI, M. P., ROGERS, J. C., KUHN, K., PIKE, I., GROTHE, R. A., BLETHROW, J. D., AND GYGI, S. P. Increasing the multiplexing capacity of TMTs using reporter ion isotopologues with isobaric masses. *Analytical Chemistry 84*, 17 (Sept. 2012), 7469–7478.

33. MI, H., MURUGANUJAN, A., EBERT, D., HUANG, X., AND THOMAS, P. D. PANTHER version 14: more genomes, a new PANTHER GO-slim and improvements in enrichment analysis tools. *Nucleic Acids Research 47*, D1 (Jan. 2019), D419–D426. Publisher: Oxford Academic.

34. MILO, R., SHEN-ORR, S., ITZKOVITZ, S., KASHTAN, N., CHKLOVSKII, D., AND ALON, U. Network Motifs: Simple Building Blocks of Complex Networks. *Science 298*, 5594 (Oct. 2002), 824–827. Publisher: American Association for the Advancement of Science Section: Report.

35. MOLL, P., ANTE, M., SEITZ, A., AND REDA, T. QuantSeq 3 mRNA sequencing for RNA quantification. *Nature Methods 11*, 12 (Dec. 2014), i–iii. Number: 12 Publisher: Nature Publishing Group.

36. NAM, K. H., AND LI, J. BRI1/BAK1, a Receptor Kinase Pair Mediating Brassinosteroid Signaling. *Cell 110*, 2 (July 2002), 203–212.

37. NASCIMENTO, M., SILVA, F. F. e., SÁFADI, T., NASCIMENTO, A. C. C., FERREIRA, T. E. M., BARROSO, L. M. A., AZEVEDO, C. F., GUIMARÃES, S. E. F., AND SERÃO, N. V. L. Independent Component Analysis (ICA) based-clustering of temporal RNA-seq data. *PLOS ONE 12*, 7 (July 2017), e0181195. Publisher: Public Library of Science.

38. NOLAN, T., CHEN, J., AND YIN, Y. Cross-talk of Brassinosteroid signaling in controlling growth and stress responses. *Biochemical Journal 474*, 16 (Aug. 2017), 2641–2661. Publisher: Portland Press.

39. NOLAN, T. M., VUKAŠINOVIĆ, N., LIU, D., RUSSINOVA, E., AND YIN, Y. Brassinosteroids: Multidimensional Regulators of Plant Growth, Development, and Stress Responses. *The Plant Cell 32*, 2 (Feb. 2020), 295–318. Publisher: American Society of Plant Biologists Section: Review.

40. OH, E., ZHU, J.-Y., BAI, M.-Y., ARENHART, R. A., SUN, Y., AND WANG, Z.-Y. Cell elongation is regulated through a central circuit of interacting transcription factors in the Arabidopsis hypocotyl. *eLife 3* (May 2014), e03031. Publisher: eLife Sciences Publications, Ltd.

41. PLANAS-RIVEROLA, A., GUPTA, A., BETEGÓN-PUTZE, I., BOSCH, N., IBAÑES, M., AND CAÑO-DELGADO, A. I. Brassinosteroid signaling in plant development and adaptation to stress. *Development 146*, 5 (Mar. 2019). Publisher: Oxford University Press for The Company of Biologists Limited Section: REVIEW.

42. PLUBELL, D. L., WILMARTH, P. A., ZHAO, Y., FENTON, A. M., MINNIER, J., REDDY, A. P., KLIMEK, J., YANG, X., DAVID, L. L., AND PAMIR, N. Extended Multiplexing of Tandem Mass Tags (TMT) Labeling Reveals Age and High Fat Diet Specific Proteome Changes in Mouse Epididymal Adipose Tissue. *Molecular & Cellular Proteomics 16*, 5 (May 2017), 873–890. Publisher: American Society for Biochemistry and Molecular Biology Section: Research.

43. RINNONE, F., MICALE, G., BONNICI, V., BADER, G. D., SHASHA, D., FERRO, A., PULVIRENTI, A., AND GIUGNO, R. NetMatchStar: an enhanced Cytoscape network querying app. *F1000Research 4* (Nov. 2015), 479.

44. SCHMIDLIN, T., DEBETS, D. O., GELDER, C. A. G. H. v., STECKER, K. E., RONTOGIANNI, S., ESHOF, B. L. v. d., KEMPER, K., LIPS, E. H., BIGGELAAR, M. v. d., PEEPER, D. S., HECK, A. J. R., AND

45. ALTELAAR, M. High-Throughput Assessment of Kinome-wide Activation States. *Cell Systems 9*, 4 (Oct. 2019), 366–374.e5. Publisher: Elsevier.

45. SHANNON, P., MARKIEL, A., OZIER, O., BALIGA, N. S., WANG, J. T., RAMAGE, D., AMIN, N., SCHWIKOWSKI, B., AND IDEKER, T. Cytoscape: a software environment for integrated models of biomolecular interaction networks. *Genome Research 13*, 11 (Nov. 2003), 2498–2504.

46. SONG, G., BRACHOVA, L., NIKOLAU, B. J., JONES, A. M., AND WALLEY, J. W. Heterotrimeric G-Protein-Dependent Proteome and Phosphoproteome in Unstimulated Arabidopsis Roots. *PROTEOMICS 18*, 24 (Dec. 2018), 1800323. Publisher: John Wiley & Sons, Ltd.

47. SONG, G., HSU, P. Y., AND WALLEY, J. W. Assessment and Refinement of Sample Preparation Methods for Deep and Quantitative Plant Proteome Profiling. *PROTEOMICS 18*, 17 (Sept. 2018), 1800220. Publisher: Wiley-Blackwell.

48. SONG, G., MONTES, C., AND WALLEY, J. W. Quantitative Profiling of Protein Abundance and Phosphorylation State in Plant Tissues Using Tandem Mass Tags. In *Plant Proteomics: Methods and Protocols*, J. V. Jorrin-Novo, L. Valledor, M. A. Castillejo, and M.-D. Rey, Eds., Methods in Molecular Biology. Springer US, New York, NY, 2020, pp. 147–156.

49. SUN, Y., FAN, X.-Y., CAO, D.-M., TANG, W., HE, K., ZHU, J.-Y., HE, J.-X., BAI, M.-Y., ZHU, S., OH, E., PATIL, S., KIM, T.-W., JI, H., WONG, W. H., RHEE, S. Y., AND WANG, Z.-Y. Integration of Brassinosteroid Signal Transduction with the Transcription Network for Plant Growth Regulation in Arabidopsis. *Developmental Cell 19*, 5 (Nov. 2010), 765–777.

50. TANG, W., KIM, T.-W., OSES-PRIETO, J. A., SUN, Y., DENG, Z., ZHU, S., WANG, R., BURLINGAME, A. L., AND WANG, Z.-Y. BSKs Mediate Signal Transduction from the Receptor Kinase BRI1 in Arabidopsis. *Science 321*, 5888 (July 2008), 557–560. Publisher: American Association for the Advancement of Science Section: Report.

51. TRAPNELL, C., ROBERTS, A., GOFF, L., PERTEA, G., KIM, D., KELLEY, D. R., PIMENTEL, H., SALZBERG, S. L., RINN, J. L., AND PACHTER, L. Differential gene and transcript expression analysis of RNA-seq experiments with TopHat and Cufflinks. *Nature Protocols 7*, 3 (Mar. 2012), 562–578. Number: 3 Publisher: Nature Publishing Group.

52. TYANOVA, S., TEMU, T., AND COX, J. The MaxQuant computational platform for mass spectrometry-based shotgun proteomics. *Nature Protocols 11*, 12 (Dec. 2016), 2301–2319.

53. VILARRASA-BLASI, J., GONZÁLEZ-GARCÍA, M.-P., FRIGOLA, D., FÀBREGAS, N., ALEXIOU, K., LÓPEZ-BIGAS, N., RIVAS, S., JAUNEAU, A., LOHMANN, J., BENFEY, P., IBAÑES, M., AND CAÑO-DELGADO, A. Regulation of Plant Stem Cell Quiescence by a Brassinosteroid Signaling Module. *Developmental Cell 30*, 1 (July 2014), 36–47.

54. WALLEY, J. W., SARTOR, R. C., SHEN, Z., SCHMITZ, R. J., WU, K. J., URICH, M. A., NERY, J. R., SMITH, L. G., SCHNABLE, J. C., ECKER, J. R., AND BRIGGS, S. P. Integration of omic networks in a developmental atlas of maize. *Science 353*, 6301 (Aug. 2016), 814–818. Publisher: American Association for the Advancement of Science Section: Report.

55. WALLEY, J. W., SHEN, Z., SARTOR, R., WU, K. J., OSBORN, J., SMITH, L. G., AND BRIGGS, S. P. Reconstruction of protein networks from an atlas of maize seed proteotypes. *Proceedings of the National Academy of Sciences 110*, 49 (Dec. 2013), E4808–E4817. Publisher: National Academy of Sciences Section: PNAS Plus.

56. WANG, G., KONG, H., SUN, Y., ZHANG, X., ZHANG, W., ALTMAN, N., dePAMPHILIS, C. W., AND MA, H. Genome-Wide Analysis of the Cyclin Family in Arabidopsis and Comparative Phylogenetic Analysis of Plant Cyclin-Like Proteins. *Plant Physiology 135*, 2 (June 2004), 1084–1099.

57. WANG, Z.-Y., NAKANO, T., GENDRON, J., HE, J., CHEN, M., VAFEADOS, D., YANG, Y., FUJIOKA, S., YOSHIDA, S., ASAMI, T., AND CHORY, J. Nuclear-Localized BZR1 Mediates Brassinosteroid-

Induced Growth and Feedback Suppression of Brassinosteroid Biosynthesis. *Developmental Cell 2*, 4 (Apr. 2002), 505–513.

58. XIANG, L., NOLAN, T. M., BAO, Y., ELMORE, M., TUEL, T., GAI, J., SHAH, D., HUSER, N. M., HURD, A. M., MCLAUGHLIN, S. A., HOWELL, S. H., WALLEY, J. W., YIN, Y., AND TANG, L. Robotic Assay for Drought (RoAD): An Automated Phenotyping System for Brassinosteroid and Drought Response. *bioRxiv* (June 2020), 2020.06.01.128199. Publisher: Cold Spring Harbor Laboratory Section: New Results.

59. XIE, Z., NOLAN, T., JIANG, H., TANG, B., ZHANG, M., LI, Z., AND YIN, Y. The AP2/ERF Transcription Factor TINY Modulates Brassinosteroid-Regulated Plant Growth and Drought Responses in Arabidopsis. *The Plant Cell 31*, 8 (Aug. 2019), 1788–1806. Publisher: American Society of Plant Biologists Section: Research Article.

60. XU, W., HUANG, J., LI, B., LI, J., AND WANG, Y. Is kinase activity essential for biological functions of BRI1? *Cell Research 18*, 4 (Apr. 2008), 472–478. Number: 4 Publisher: Nature Publishing Group.

61. YE, H., LIU, S., TANG, B., CHEN, J., XIE, Z., NOLAN, T. M., JIANG, H., GUO, H., LIN, H.-Y., LI, L., WANG, Y., TONG, H., ZHANG, M., CHU, C., LI, Z., ALURU, M., ALURU, S., SCHNABLE, P. S., AND YIN, Y. RD26 mediates crosstalk between drought and brassinosteroid signalling pathways. *Nature Communications 8*, 1 (Feb. 2017), 14573. Number: 1 Publisher: Nature Publishing Group.

62. YIN, Y., VAFEADOS, D., TAO, Y., YOSHIDA, S., ASAMI, T., AND CHORY, J. A New Class of Transcription Factors Mediates Brassinosteroid-Regulated Gene Expression in Arabidopsis. *Cell 120*, 2 (Jan. 2005), 249–259.

63. YIN, Y., WANG, Z.-Y., MORA-GARCIA, S., LI, J., YOSHIDA, S., ASAMI, T., AND CHORY, J. BES1 Accumulates in the Nucleus in Response to Brassinosteroids to Regulate Gene Expression and Promote Stem Elongation. *Cell 109*, 2 (Apr. 2002), 181–191.

64. YU, X., LI, L., ZOLA, J., ALURU, M., YE, H., FOUDREE, A., GUO, H., ANDERSON, S., ALURU, S., LIU, P., RODERMEL, S., AND YIN, Y. A brassinosteroid transcriptional network revealed by genome-wide identification of BESI target genes in Arabidopsis thaliana. *The Plant Journal 65*, 4 (2011), 634–646. _eprint: https://onlinelibrary.wiley.com/doi/pdf/10.1111/j.1365-313X.2010.04449.x.

65. ZANDER, M., LEWSEY, M. G., CLARK, N. M., YIN, L., BARTLETT, A., SALDIERNA GUZMÁN, J. P., HANN, E., LANGFORD, A. E., JOW, B., WISE, A., NERY, J. R., CHEN, H., BAR-JOSEPH, Z., WALLEY, J. W., SOLANO, R., AND ECKER, J. R. Integrated multi-omics framework of the plant response to jasmonic acid. *Nature Plants 6*, 3 (Mar. 2020), 290–302. Number: 3 Publisher: Nature Publishing Group.

66. ZHAO, J., PENG, P., SCHMITZ, R. J., DECKER, A. D., TAX, F. E., AND LI, J. Two Putative BIN2 Substrates Are Nuclear Components of Brassinosteroid Signaling. *Plant Physiology 130*, 3 (Nov. 2002), 1221–1229. Publisher: American Society of Plant Biologists Section: CELL BIOLOGY AND SIGNAL TRANSDUCTION.

67. ZHOU, X.-Y., SONG, L., AND XUE, H.-W. Brassinosteroids Regulate the Differential Growth of Arabidopsis Hypocotyls through Auxin Signaling Components IAA19 and ARF7. *Molecular Plant 6*, 3 (May 2013), 887–904.